AIP Advances

Spectromicroscopic measurements of electronic structure variations in atomically thin WSe_2

Cite as: AIP Advances **10**, 095027 (2020); https://doi.org/10.1063/5.0018639
Submitted: 20 August 2020 . Accepted: 28 August 2020 . Published Online: 28 September 2020

T. Klaproth, C. Habenicht, R. Schuster, B. Büchner, M. Knupfer, and A. Koitzsch

COLLECTIONS

Paper published as part of the special topic on Chemical Physics, Energy, Fluids and Plasmas, Materials Science and Mathematical Physics

View Online Export Citation CrossMark

ARTICLES YOU MAY BE INTERESTED IN

Numerical investigations of trajectory characteristics of a high-speed water-entry projectile
AIP Advances **10**, 095107 (2020); https://doi.org/10.1063/5.0011308

Structural, electronic, and transport properties of Co-, Cr-, and Fe-doped functionalized armchair MoS_2 nanoribbons
AIP Advances **10**, 095029 (2020); https://doi.org/10.1063/5.0022891

Origin of band inversion in topological Bi_2Se_3
AIP Advances **10**, 095018 (2020); https://doi.org/10.1063/5.0022525

© 2020 Author(s).

Spectromicroscopic measurements of electronic structure variations in atomically thin WSe_2

Cite as: AIP Advances 10, 095027 (2020); doi: 10.1063/5.0018639
Submitted: 20 August 2020 • Accepted: 28 August 2020 •
Published Online: 28 September 2020

View Online Export Citation CrossMark

T. Klaproth,[1] C. Habenicht,[1] R. Schuster,[1] B. Büchner,[1,2] M. Knupfer,[1] and A. Koitzsch[1,a)]

AFFILIATIONS

[1] IFW Dresden, Helmholtzstraße 20, 01069 Dresden, Germany
[2] Institute of Solid State and Materials Physics, TU Dresden, 01069 Dresden, Germany

[a)] Author to whom correspondence should be addressed: a.koitzsch@ifw-dresden.de

ABSTRACT

Atomically thin transition metal dichalcogenides (TMDCs) are promising candidates for implementation in next generation semiconducting devices, for which laterally homogeneous behavior is needed. Here, we study the electronic structure of atomically thin exfoliated WSe_2, a prototypical TMDC with large spin–orbit coupling, by photoemission electron microscopy, electron energy-loss spectroscopy, and density functional theory. We resolve the inhomogeneities of the doping level by the varying energy positions of the valence band. There appear to be different types of inhomogeneities that respond differently to electron doping, introduced by potassium intercalation. In addition, we find that the doping process itself is more complex than previously anticipated and entails a distinct orbital and thickness dependence that needs to be considered for effective band engineering. In particular, the density of selenium vs tungsten states depends on the doping level, which leads to changes in the optical response beyond increased dielectric screening. Our work gives insight into the inhomogeneity of the electron structure of WSe_2 and the effects of electron doping, provides microscopic understanding thereof, and improves the basis for property engineering of 2D materials.

© 2020 Author(s). All article content, except where otherwise noted, is licensed under a Creative Commons Attribution (CC BY) license (http://creativecommons.org/licenses/by/4.0/). https://doi.org/10.1063/5.0018639

I. INTRODUCTION

Semiconducting transition metal dichalcogenides (TMDCs) such as MoS_2 and WSe_2 have attracted enormous scientific attention in the last years.[1] Their layered crystal structure allows downsizing them to single atomic layers without dangling bonds, which can be functionalized in electronic devices with promising performance parameters. This meets the desire to find electronically active materials that may substitute silicon at the extreme miniaturization limit.[2] Field effect transistors based on atomically thin MoS_2 and WSe_2 as channel materials with excellent switching characteristics[3] and high mobility[4,5] have been demonstrated. Moreover, TMDCs exhibit various other intriguing physical properties holding strong potential for optoelectronic applications, such as thickness dependent bandgaps in the visible energy range[6,7] and the locking of spin and momentum at the K/K' valleys giving rise to the field of valleytronics.[8,9]

WSe_2, in particular, possesses several advantages compared to other TMDCs. It is easier to control the character of the charge carriers ranging from hole dominated, ambipolar to electron dominated.[10,11] Moreover, the spin–orbit coupling is larger than that in MoS_2, making WSe_2 especially suitable for studying spin and valley dependent properties.

The great success of silicon as the backbone of semiconducting industry roots partially in the ability to precisely control its properties by alloying, implantation or diffusion of dopant ions, and maintaining high levels of homogeneity. Similar methods of band engineering are needed for TMDCs. Indeed, several attempts have been reported in this regard,[12,13] e.g., controlled defect creation by sputtering or thermal treatments,[14,15] substitution with dopants, e.g., Nb,[16,17] isovalent substitution of the type $WSe_{1-x}S_x$,[18,19] and charge transfer doping by donor or acceptor atoms or molecules.[20] The latter is achieved by solution based methods or by *in situ* evaporation of the pertinent dopant material. It is a well established method for layered materials and has been applied to bulk TMDCs and graphite among others. Alkali metals figure prominently as donors and, among the alkali metals, potassium offers probably the highest

© Author(s) 2020

degree of electron transfer. It has been repeatedly used to achieve n type doping in atomically thin MoS_2 and WSe_2 up to degenerate doping levels and the transition to a metallic state.[21,22] The latter has been directly monitored by angle-resolved photoemission spectroscopy (ARPES) by the observation of the electron pockets.[23–26] Apart from providing electrons, potassium may introduce defects or alter the existing ones.[27] It may also affect the lateral homogeneity of the doping level.

Spatial inhomogeneities play an important role for the properties of TMDCs and much work has been devoted to them.[28–35] Inhomogeneities may originate from different sources, such as intrinsic defects and doping variations, strain, and dielectric disorder.[36,37] An important consequence is the local fluctuation of the Fermi level with respect to the gap edges, which determines band alignment.

Here, we measure the valence band with lateral resolution, extract the energy landscape of its position, and determine how it evolves upon electron doping. For controlled band and defect engineering, it is crucial to understand the effects of doping beyond simple band filling taking into account lateral inhomogeneities and chemical modifications. To this end, we utilize photoemission electron microscopy (PEEM), electron energy-loss spectroscopy (EELS), and density functional theory (DFT) and obtain a comprehensive picture of the electronic structure of exfoliated, atomically thin WSe_2.

II. METHODS

2H-WSe_2 single crystals have been purchased from HQ graphene and exfoliated down to a single layer using polydimethylsiloxane (PDMS) sheets. The WSe_2 flakes were transferred to a silicon substrate with an oxide thickness of 90 nm. To avoid charging effects during photoemission experiments, the substrate is coated with a 10 nm gold layer. The optical contrast is sufficient to distinguish single layer differences.

Atomic force microscopy (AFM) measurements were carried out using a Bruker Dimension Icon microscope in tapping mode. Since photoemission experiments are highly surface sensitive, the characterization via AFM was done after the photoemission measurements, including the doping experiments resulting in rather rough surface profiles. The results of the AFM measurements are shown in the supplementary material.

The photoemission data were measured using a NanoESCA system (Scienta Omicron) equipped with a helium lamp with an energy of 21.21 eV (He I) and an energy resolution of ≤0.2 eV. The spatial resolution is below 1 μm.

After obtaining an initial photoemission dataset of the freshly exfoliated flake, potassium was deposited onto the flake in steps using the SAES dispensers. The deposition rate was controlled by a quartz crystal microbalance and found to be about 0.2 nm/min.

The EELS measurements were carried out using a purpose built transmission electron energy-loss spectrometer with a primary electron energy of 172 keV and the energy and momentum resolution of $\Delta E = 82$ meV and $\Delta q = 0.04$ Å^{-1}, respectively, at $T = 20$ K.[38,39] The films (*thickness* ≈ 100 nm) were exfoliated using a scotch tape. Subsequently, the films were mounted onto standard electron microscopy grids and transferred into the EELS spectrometer. The undoped crystals were intercalated *in situ* by potassium vapor from the SAES dispensers.

The band structure calculations were performed using the full-potential local-orbital code (FPLO)[40] employing the Perdew-Wang 92 exchange-correlation-functional.[41] For 1-layer to 4-layer WSe_2, we constructed super-cells with about 10 nm of vacuum between layers and sampled the Brillouin zone with a (18 × 18 × 1) k-point mesh. For bulk WSe_2, a (12 × 12 × 12) k-point mesh was used. Only the lattice constant a was optimized by minimizing the total energy of bulk-WSe_2 and was found to be $a = 3.302$ Å. The parameter c was set to the experimental value of 12.982 Å[42] since van der Waals interactions are not taken into account. The lattice constants determined in this way were used for the 1-layer to 4-layer calculations as well. All calculations were performed in fully relativistic mode. The calculations have been performed for freestanding flakes, i.e., no interaction with the substrate is taken into account.

III. RESULTS AND DISCUSSION

An optical microscope image of the prepared flake is given in Fig. 1(a). Figure 1(c) shows the same flake measured by photoemission electron microscopy (PEEM) at four different energies. The areas of different thicknesses can be distinguished in the images. From atomic force microscopy and photoemission spectroscopy (PES) measurements, we conclude that area 1 corresponds to a monolayer, area 2 to a trilayer, and area 3 to a four layer. X-ray photoemission spectroscopy of the Se 3d and W 4f core levels confirms the absence of oxides and other foreign phases. See the supplementary material for further information and additional AFM, PEEM, and XPS data.

A. Doping homogeneity

We start by considering the homogeneity of the electronic structure. In order to do so, we apply PEEM to measure the valence band laterally resolved at all positions of the flake. The inset of Fig. 2(a) presents the low energy part of the monolayer valence band integrated around the Γ point. The energy location of the valence band depends on the position of the Fermi energy inside the gap and represents a signature of the doping level. The position of the leading peak can be evaluated by standard fitting procedures (see the supplementary material for details). Figures 2(a)–2(d) show these positions for the monolayer region of the flake evaluated by pixel-by-pixel analysis before and after potassium intercalation. Figure 4 of the supplementary material presents some explicit examples of the spectra and fitting curves, confirming the high quality and reliability of the fitting procedure. Note that the valence band maximum of the monolayer is situated at K rather than Γ (see Fig. 2 of the supplementary material). However, here, we are interested in the relative changes in the energy rather than the absolute values of the valence band maxima.

Figures 2(a) and 2(c) show the valence band positions of the undoped and doped flakes on a joint color scale, whereas Figs. 2(b) and 2(d) maximize the local contrast by applying separate scales to the same data. The map of the undoped sample, indeed, shows inhomogeneities on the μm scale with the energy variations in the order of 50 meV. The overall effect of potassium intercalation is a shift to lower energy [Figs. 2(a) and 2(c)]. This is expected because of

© Author(s) 2020

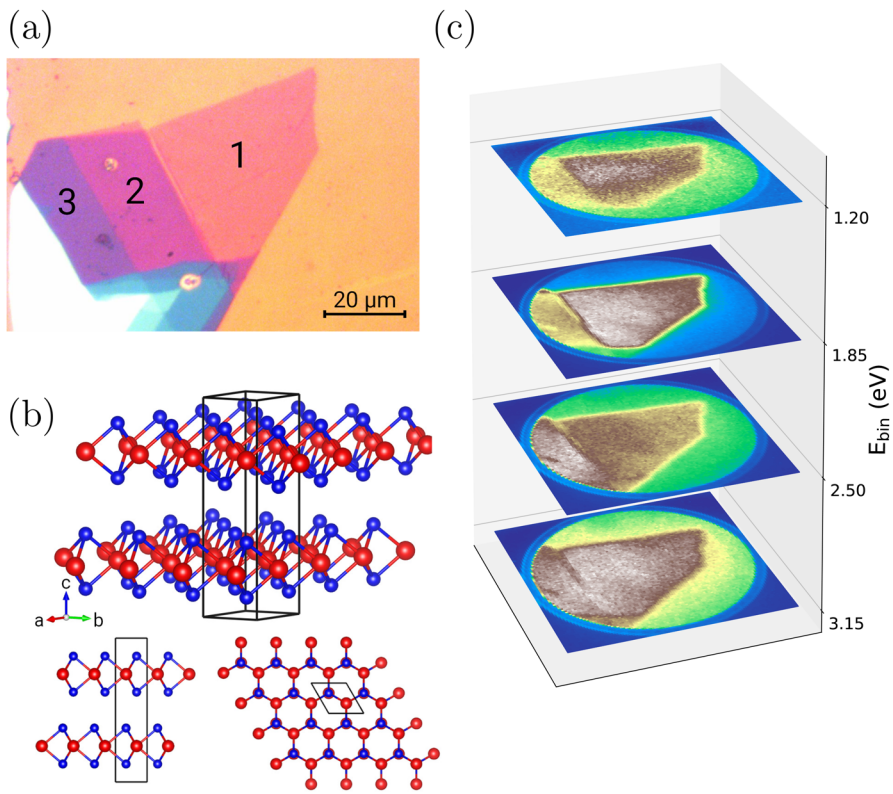

FIG. 1. (a) Optical microscope image of the investigated flake on the substrate. (b) Crystal structure of WSe_2. (c) Photoemission intensity distributions of the right part of the flake at different binding energies. The areas 1 and 2 can be distinguished.

the well known *n* type character of alkali metal intercalation.[25,26,43] A closer inspection of Figs. 2(b) and 2(d) reveals that the shift is not uniform. In particular, the contrast of some elongated, stripe-like structures increases and they become generally more prominent. This impression is confirmed by examining the valence band position along the white dashed lines in Figs. 2(b) and 2(d), as shown in Fig. 2(f). The energy difference, i.e., the contrast, across the elongated structure becomes larger with doping (purple shaded region). On the other hand, the contrast decreases in the turquoise shaded region, where a more regular patch-like structure is situated for the undoped sample. Hence, the response of the electronic structure for these two regions is qualitatively different.

The histograms of the energy position for the undoped and doped cases are depicted in Fig. 2(e). The overall shift amounts to $\Delta E = 0.22$ eV. The error of the individual fits is well below the width of the histograms. Hence, the histograms represent the intrinsic distribution of the valence band positions. A laterally integrated spectrum may acquire additional broadening due to this inhomogeneity.

We interpret the two-fold response of the Fermi level position on electron doping as a consequence of different types of inhomogeneity, whereas the elongated, stripe like structures are possibly related to the microcracks introduced by the exfoliation transfer process, and the patches could be due to the variations of dielectric screening imposed by the local flake–substrate interaction. It has been shown previously that edges and microcracks are more easily functionalized by extrinsic manipulations than the smooth inner part of the flake.[44–46] The edge sites probably are chemically more reactive. This increases the inhomogeneity upon potassium intercalation. Local dielectric fluctuations, on the other hand, are expected to be smoothened when immersed in an additional charge reservoir, which increases screening.

Electron doping by potassium intercalation causes specific effects not only depending on the type of underlying inhomogeneity but also depending on the thickness and with respect to the involved atomic orbital character.

B. Suppression of the Se states

Figure 3 presents valence band photoemission spectra taken from the monolayer, the trilayer, and the tetralayer before and after doping. The momentum window is again restricted to the vicinity of the Γ point. The shape of the spectra depends on the number of layers. The leading peaks of the trilayer and four-layer spectra do not correspond to the first peaks of the density of states (DOS) because the photoemission intensity of the uppermost bands is weak and hidden below the tails of the main peak at $E \approx 2$ eV (see Fig. S3).

When applying potassium intercalation to the sample, several changes of the electronic structure are observed. First of all, the intercalated spectra shift to lower energy for all thicknesses. For a sufficiently large potassium concentration, the conduction band would eventually become occupied and an insulator–metal transition occurs.[44,47–49] The thickness dependent energy shifts are discussed in detail below. Here, we focus on the changes of the spectral shape. In particular, there are well resolved peaks highlighted by

© Author(s) 2020

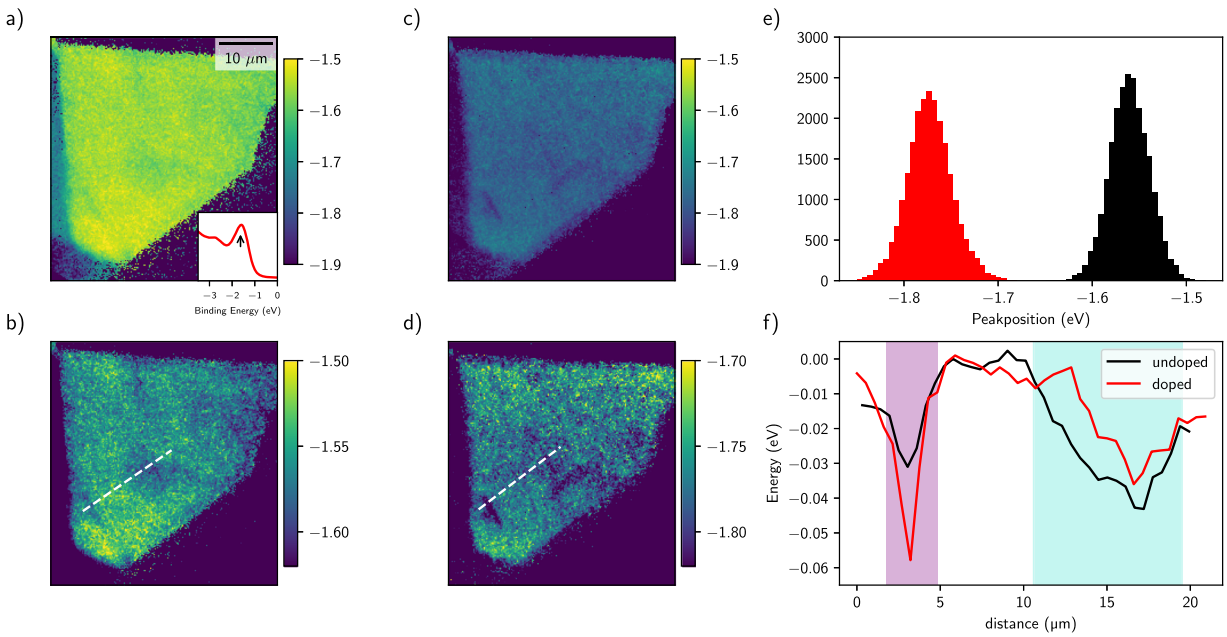

FIG. 2. (a) Valence band position of the undoped flake. Inset: integrated valence band around Γ. (b) Valence band position of the undoped flake with a zoomed color scale. The white line indicated the position of the line scan in (f). (c) Valence band position of the doped flake. (d) Valence band position of the undoped flake with the zoomed color scale. (e) Histograms of the valence band positions of undoped (black) and doped (red) flake. (f) Line scan of the valence band position along the white dashed line in (b) and (d). Black: undoped and red: doped. The purple and turquoise shadings are discussed in the text.

arrows for the undoped sample that vanish or become significantly less intense upon doping. We associate the origin of this effect to the orbital character of the involved bands. In the lower part of Fig. 3, we depict the orbital resolved density of states (pDOS) calculated for the undoped material. In order to facilitate meaningful comparison to the experimental data, we restricted k-integration of the DOS to the same window that applies for experiment ($\Delta k \approx 0.15$ Å).

The leading peaks are dominated by the tungsten states in each case. The smaller peaks indicated by arrows in Fig. 3 are mostly formed by the Se states. We conclude that the potassium intercalation disturbs the Se lattice more profoundly than the W sublattice. This is naturally explained by the sandwich type monolayer structure where the middle W layer is protected by the outer Se layers. It is also consistent with the previous DFT studies, which show that a chemical bond between Se and K is established.[21,50] The tungsten lattice and the tungsten states appear to be intrinsically protected, which is important because the uppermost valence band is dominated by W 5*d*.

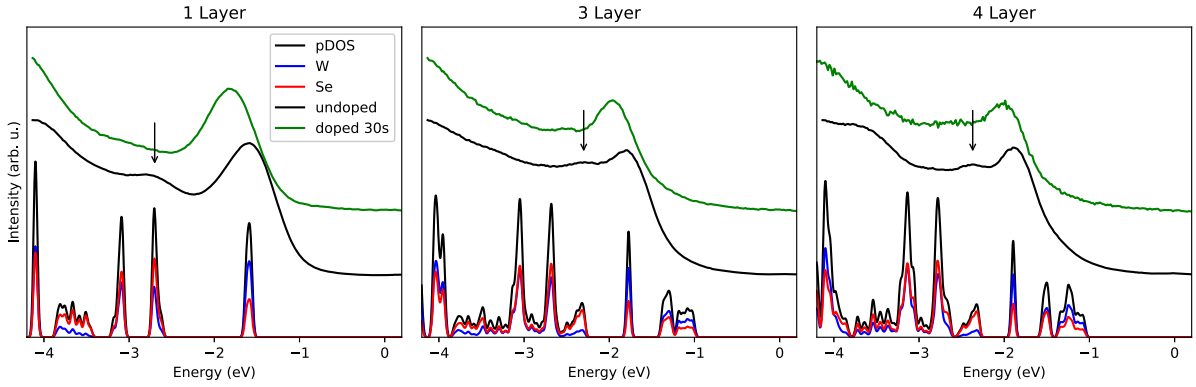

FIG. 3. Comparison of doped and undoped photoemission spectra integrated around Γ and partial density of states as a function of the number of layers.

© Author(s) 2020

If the Se-related pDOS is modified by potassium intercalation, other material properties should be affected. Of particular importance for the TMDC are the optical properties that depend on the electronic structure and must be influenced by the purported scenario.[6,7] Therefore, we investigated the dielectric properties of potassium doped WSe_2 by EELS in the optical limit, i.e., momentum transfer near zero. Figure 4 shows EELS measurements of undoped (a) and doped (b) bulk samples.[51] The undoped sample is gapped below ~1.7 eV followed by a sharp intensity onset and a peak at $E = 1.8$ eV. This peak is of excitonic character.[47,52,53] The structures at higher energies are due to interband transitions but may also be influenced by excitonic effects. The doped sample is metallic, as can be seen by the presence of the charge carrier plasmon at $E \approx 1$ eV.[51] No exciton is present anymore, as expected for the metallic samples, and the spectral shape at higher energies has changed with respect to the undoped case.

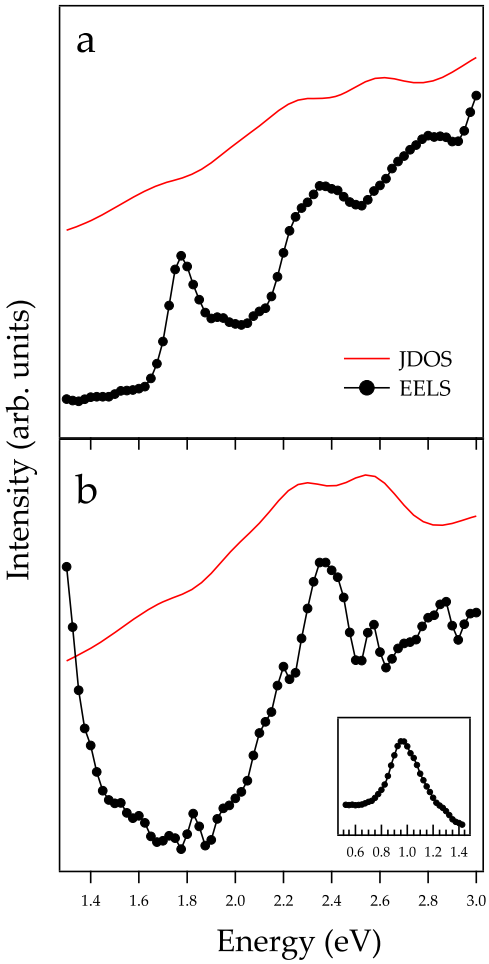

FIG. 4. Experimental EELS data for (a) undoped and (b) doped WSe_2 in its bulk form. The red line represents the joint density of states, which accounts for the higher lying features and their doping dependence. Inset: low energy region of the doped sample covering the charge carrier plasmon.

In order to understand these changes and to connect the EELS results with the PES measurements above, we compare the EELS measurements with the joint density of states (JDOS) in Fig. 4. The JDOS is proportional to the imaginary part of the dielectric function $\epsilon_2(\omega)$, which is an approximate measure of the so-called loss function, determining EELS intensity. At the same time, $\epsilon_2(\omega)$ is responsible for the optical absorption. The JDOS has been calculated based on the DFT results shown in Fig. 3 and shifted by 0.9 eV to lower energy for better comparison with experiment. The JDOS derived in this way relies on the one-particle band structure and cannot reproduce the intense exciton at 1.8 eV correctly. However, at higher energies, our model matches qualitatively the experimental results and the doping dependence. The JDOS for the doped sample was calculated in the following way: motivated by the reduced Se photoemission intensity after potassium deposition, we weighted the JDOS by the tungsten orbital weight at each k-point, which means that the Se derived states are suppressed. The downturn at $E = 2.6$ eV–2.8 eV in Fig. 4(b) corresponds to this suppression of the Se bands analogous to the doping dependence of the EDCs in Fig. 3.

The effect of potassium doping on the optical properties can be summarized as follows: it reduces excitonic effects by enhancing the screening of many body interactions. From a rigorous treatment, which involved the Kramers–Kronig analysis of EELS data of an equivalent sample, we obtained previously an electron density of 1.2 e^-/u.c.[51] In addition, the underlying interband transitions themselves are altered in an energy range that is still accessible by visible light.

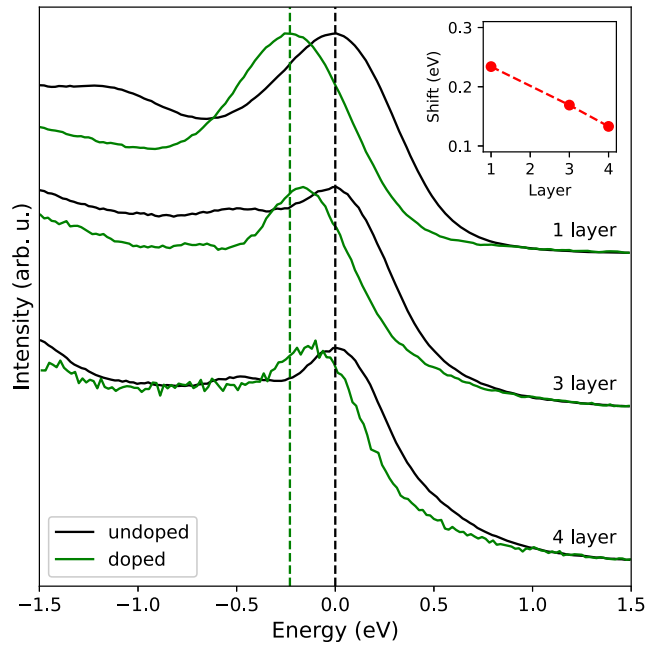

FIG. 5. Comparison of undoped and doped photoemission spectra integrated around Γ as a function of the number of layers. The leading peaks have been aligned for the undoped samples of different thicknesses in order to highlight the position dependence of the doped case. Inset: energy shift as a function of thickness.

© Author(s) 2020

C. Thickness dependence

The electron doping generally causes an upward shift of the Fermi level. Now, we consider the thickness dependence of this shift. Figure 5 collects the photoemission spectra of Fig. 3 on a joint energy axis and aligns the leading peak of the undoped spectra for each thickness. The corresponding doped spectra are shifted accordingly. From this representation, it becomes clear that the energy shift depends on thickness. The difference of the peak position is maximal for the monolayer and decreases for the three layer and four layer samples.

The amount of potassium evaporated per unit area is exactly the same in each case. The effective doping per sample volume, on the other hand, will be lower for the thicker parts of the sample. Hence, the shift of the Fermi level is smaller. This means that the band alignment of adjacent layers of different thicknesses depends on the doping level applied. Such lateral homojunctions have been studied before. A monolayer–bilayer junction features a type I band alignment accompanied by band bending near the interface.[54–58] Alkali metal intercalation represents a means of engineering the valence band offset at such junctions. However, it follows from Sec. III A that the interface region itself would be modified even stronger than the inner regions of the films.

IV. CONCLUSIONS

We measured the electronic structure of atomically thin WSe_2 by PEEM, EELS, and DFT. Lateral inhomogeneity is observed, which spans an energy scale of ~50 meV and a length scale of μm. Electron doping by potassium intercalation affects the electronic structure in various ways. It increases the inhomogeneity; especially along the stripe-like regions possibly related to the microcracks or domain walls, it suppresses the Se states, which means that the sample is chemically modified, and it alters the thickness dependent valence band offset across the flake. These changes have an effect on the optical properties that goes beyond enhanced dielectric screening.

SUPPLEMENTARY MATERIAL

See the supplementary material for (i) AFM measurements, (ii) further valence band photoemission data, including angle-resolved measurements, a detailed description of the fitting procedure underlying Fig. 2 and example spectra, and (iii) XPS data.

ACKNOWLEDGMENTS

We thank R. Hübel, S. Leger, F. Thunig, and M. Naumann for technical and Ulrike Nitzsche for computational assistance. This work was supported by the German Research Foundation (DFG) under Grant No. SFB 1143.

DATA AVAILABILITY

The data that support the findings of this study are available from the corresponding author upon reasonable request.

REFERENCES

[1] S. Manzeli, D. Ovchinnikov, D. Pasquier, O. V. Yazyev, and A. Kis, "2D transition metal dichalcogenides," Nat. Rev. Mater. **2**, 17033 (2017).
[2] J. A. Robinson, "Perspective: 2D for beyond CMOS," APL Mater. **6**, 058202 (2018).
[3] S. B. Desai, S. R. Madhvapathy, A. B. Sachid, J. P. Llinas, Q. Wang, G. H. Ahn, G. Pitner, M. J. Kim, J. Bokor, C. Hu, H. S. P. Wong, and A. Javey, "MoS_2 transistors with 1-nanometer gate lengths," Science **354**, 99–102 (2016).
[4] B. Radisavljevic, A. Radenovic, J. Brivio, V. Giacometti, and A. Kis, "Single-layer MoS_2 transistors," Nat. Nanotechnol. **6**, 147 EP (2011).
[5] H.-J. Chuang, X. Tan, N. J. Ghimire, M. M. Perera, B. Chamlagain, M. M.-C. Cheng, J. Yan, D. Mandrus, D. Tománek, and Z. Zhou, "High mobility WSe_2 *p*- and *n*-type field-effect transistors contacted by highly doped graphene for low-resistance contacts," Nano Lett. **14**, 3594–3601 (2014).
[6] K. F. Mak, C. Lee, J. Hone, J. Shan, and T. F. Heinz, "Atomically thin MoS_2: A new direct-gap semiconductor," Phys. Rev. Lett. **105**, 136805 (2010).
[7] A. Splendiani, L. Sun, Y. Zhang, T. Li, J. Kim, C.-Y. Chim, G. Galli, and F. Wang, "Emerging photoluminescence in monolayer MoS_2," Nano Lett. **10**, 1271–1275 (2010).
[8] D. Xiao, G.-B. Liu, W. Feng, X. Xu, and W. Yao, "Coupled spin and valley physics in monolayers of MoS_2 and other group-VI dichalcogenides," Phys. Rev. Lett. **108**, 196802 (2012).
[9] J. R. Schaibley, H. Yu, G. Clark, P. Rivera, J. S. Ross, K. L. Seyler, W. Yao, and X. Xu, "Valleytronics in 2D materials," Nat. Rev. Mater. **1**, 16055 (2016).
[10] H. Fang, S. Chuang, T. C. Chang, K. Takei, T. Takahashi, and A. Javey, "High-performance single layered WSe_2 *p*-FETs with chemically doped contacts," Nano Lett. **12**, 3788–3792 (2012).
[11] C. Zhou, Y. Zhao, S. Raju, Y. Wang, Z. Lin, M. Chan, and Y. Chai, "Carrier type control of WSe_2 field-effect transistors by thickness modulation and MoO_3 layer doping," Adv. Funct. Mater. **26**, 4223–4230 (2016).
[12] Z. Hu, Z. Wu, C. Han, J. He, Z. Ni, and W. Chen, "Two-dimensional transition metal dichalcogenides: Interface and defect engineering," Chem. Soc. Rev. **47**, 3100–3128 (2018).
[13] P. Luo, F. Zhuge, Q. Zhang, Y. Chen, L. Lv, Y. Huang, H. Li, and T. Zhai, "Doping engineering and functionalization of two-dimensional metal chalcogenides," Nanoscale Horiz. **4**, 26–51 (2019).
[14] S. Tongay, J. Suh, C. Ataca, W. Fan, A. Luce, J. S. Kang, J. Liu, C. Ko, R. Raghunathanan, J. Zhou, F. Ogletree, J. Li, J. C. Grossman, and J. Wu, "Defects activated photoluminescence in two-dimensional semiconductors: Interplay between bound, charged, and free excitons," Sci. Rep. **3**, 2657 (2013).
[15] Z. Wu, Z. Luo, Y. Shen, W. Zhao, W. Wang, H. Nan, X. Guo, L. Sun, X. Wang, Y. You, and Z. Ni, "Defects as a factor limiting carrier mobility in WSe_2: A spectroscopic investigation," Nano Res. **9**, 3622–3631 (2016).
[16] J. Suh, T.-E. Park, D.-Y. Lin, D. Fu, J. Park, H. J. Jung, Y. Chen, C. Ko, C. Jang, Y. Sun, R. Sinclair, J. Chang, S. Tongay, and J. Wu, "Doping against the native propensity of MoS_2: Degenerate hole doping by cation substitution," Nano Lett. **14**, 6976–6982 (2014).
[17] A. Nipane, D. Karmakar, N. Kaushik, S. Karande, and S. Lodha, "Few-layer MoS_2 *p*-type devices enabled by selective doping using low energy phosphorus implantation," ACS Nano **10**, 2128–2137 (2016).
[18] Y. Chen, J. Xi, D. O. Dumcenco, Z. Liu, K. Suenaga, D. Wang, Z. Shuai, Y.-S. Huang, and L. Xie, "Tunable band gap photoluminescence from atomically thin transition-metal dichalcogenide alloys," ACS Nano **7**, 4610–4616 (2013).
[19] X. Duan, C. Wang, Z. Fan, G. Hao, L. Kou, U. Halim, H. Li, X. Wu, Y. Wang, J. Jiang, A. Pan, Y. Huang, R. Yu, and X. Duan, "Synthesis of $WS_{2x}Se_{2-2x}$ alloy nanosheets with composition-tunable electronic properties," Nano Lett. **16**, 264–269 (2016).
[20] X. Zhang, Z. Shao, X. Zhang, Y. He, and J. Jie, "Surface charge transfer doping of low-dimensional nanostructures toward high-performance nanodevices," Adv. Mater. **28**, 10409–10442 (2016).
[21] H. Fang, M. Tosun, G. Seol, T. C. Chang, K. Takei, J. Guo, and A. Javey, "Degenerate *n*-doping of few-layer transition metal dichalcogenides by potassium," Nano Lett. **13**, 1991–1995 (2013).

© Author(s) 2020

[22]B. Lei, Y. Pan, Z. Hu, J. Zhang, D. Xiang, Y. Zheng, R. Guo, C. Han, L. Wang, J. Lu, L. Yang, and W. Chen, "Direct observation of semiconductor-metal phase transition in bilayer tungsten diselenide induced by potassium surface functionalization," ACS Nano **12**, 2070–2077 (2018).
[23]T. Eknapakul, P. D. C. King, M. Asakawa, P. Buaphet, R.-H. He, S.-K. Mo, H. Takagi, K. M. Shen, F. Baumberger, T. Sasagawa, S. Jungthawan, and W. Meevasana, "Electronic structure of a quasi-freestanding MoS_2 monolayer," Nano Lett. **14**, 1312–1316 (2014).
[24]J. M. Riley, W. Meevasana, L. Bawden, M. Asakawa, T. Takayama, T. Eknapakul, T. K. Kim, M. Hoesch, S.-K. Mo, H. Takagi, T. Sasagawa, M. S. Bahramy, and P. D. C. King, "Negative electronic compressibility and tunable spin splitting in WSe_2," Nat. Nano **10**, 1043–1047 (2015).
[25]Y. Zhang, M. M. Ugeda, C. Jin, S.-F. Shi, A. J. Bradley, A. Martín-Recio, H. Ryu, J. Kim, S. Tang, Y. Kim, B. Zhou, C. Hwang, Y. Chen, F. Wang, M. F. Crommie, Z. Hussain, Z.-X. Shen, and S.-K. Mo, "Electronic structure, surface doping, and optical response in epitaxial WSe_2 thin films," Nano Lett. **16**, 2485–2491 (2016).
[26]M. Kang, B. Kim, S. H. Ryu, S. W. Jung, J. Kim, L. Moreschini, C. Jozwiak, E. Rotenberg, A. Bostwick, and K. S. Kim, "Universal mechanism of band-gap engineering in transition-metal dichalcogenides," Nano Lett. **17**, 1610–1615 (2017).
[27]C. Zhang, C. Wang, F. Yang, J.-K. Huang, L.-J. Li, W. Yao, W. Ji, and C.-K. Shih, "Engineering point-defect states in monolayer WSe_2," ACS Nano **13**, 1595–1602 (2019).
[28]R. Addou, S. McDonnell, D. Barrera, Z. Guo, A. Azcatl, J. Wang, H. Zhu, C. L. Hinkle, M. Quevedo-Lopez, H. N. Alshareef, L. Colombo, J. W. P. Hsu, and R. M. Wallace, "Impurities and electronic property variations of natural MoS_2 crystal surfaces," ACS Nano **9**, 9124–9133 (2015).
[29]R. Addou and R. M. Wallace, "Surface analysis of WSe_2 crystals: Spatial and electronic variability," ACS Appl. Mater. Interfaces **8**, 26400–26406 (2016).
[30]D. Jariwala, A. Krayev, J. Wong, A. E. Robinson, M. C. Sherrott, S. Wang, G.-Y. Liu, M. Terrones, and H. A. Atwater, "Nanoscale doping heterogeneity in few-layer WSe_2 exfoliated onto noble metals revealed by correlated SPM and TERS imaging," 2D Mater. **5**, 035003 (2018).
[31]X. Dong, A. K. Yetisen, M. H. Köhler, J. Dong, S. Wang, M. Jakobi, X. Zhang, and A. W. Koch, "Microscale spectroscopic mapping of 2D optical materials," Adv. Opt. Mater. **7**, 1900324 (2019).
[32]R. Dagan, Y. Vaknin, A. Henning, J. Y. Shang, L. J. Lauhon, and Y. Rosenwaks, "Two-dimensional charge carrier distribution in MoS_2 monolayer and multilayers," Appl. Phys. Lett. **114**, 101602 (2019).
[33]B. R. Carvalho, Y. Wang, K. Fujisawa, T. Zhang, E. Kahn, I. Bilgin, P. M. Ajayan, A. M. de Paula, M. A. Pimenta, S. Kar, V. H. Crespi, M. Terrones, and L. M. Malard, "Nonlinear dark-field imaging of one-dimensional defects in monolayer dichalcogenides," Nano Lett. **20**, 284–291 (2020).
[34]D. Edelberg, D. Rhodes, A. Kerelsky, B. Kim, J. Wang, A. Zangiabadi, C. Kim, A. Abhinandan, J. Ardelean, M. Scully, D. Scullion, L. Embon, R. Zu, E. J. G. Santos, L. Balicas, C. Marianetti, K. Barmak, X. Zhu, J. Hone, and A. N. Pasupathy, "Approaching the intrinsic limit in transition metal diselenides via point defect control," Nano Lett. **19**, 4371–4379 (2019).
[35]C. Kastl, R. J. Koch, C. T. Chen, J. Eichhorn, S. Ulstrup, A. Bostwick, C. Jozwiak, T. R. Kuykendall, N. J. Borys, F. M. Toma, S. Aloni, A. Weber-Bargioni, E. Rotenberg, and A. M. Schwartzberg, "Effects of defects on band structure and excitons in WS_2 revealed by nanoscale photoemission spectroscopy," ACS Nano **13**, 1284–1291 (2019).
[36]K. Zhang, Y. Wang, J. Joshi, F. Zhang, S. Subramanian, M. Terrones, P. Vora, V. Crespi, and J. A. Robinson, "Probing the origin of lateral heterogeneities in synthetic monolayer molybdenum disulfide," 2D Mater. **6**, 025008 (2019).
[37]A. Raja, L. Waldecker, J. Zipfel, Y. Cho, S. Brem, J. D. Ziegler, M. Kulig, T. Taniguchi, K. Watanabe, E. Malic, T. F. Heinz, T. C. Berkelbach, and A. Chernikov, "Dielectric disorder in two-dimensional materials," Nat. Nanotechnol. **14**, 832–837 (2019).
[38]J. Fink, "Recent developments in energy-loss spectroscopy," in *Advances in Electronics and Electron Physics* (Elsevier, 1989), Vol. 75, pp. 121–232.
[39]F. Roth, A. König, J. Fink, B. Büchner, and M. Knupfer, "Electron energy-loss spectroscopy: A versatile tool for the investigations of plasmonic excitations," J. Electron Spectrosc. Relat. Phenom. **195**, 85–95 (2014).
[40]K. Koepernik and H. Eschrig, "Full-potential nonorthogonal local-orbital minimum-basis band-structure scheme," Phys. Rev. B **59**, 1743–1757 (1999).
[41]J. P. Perdew and Y. Wang, "Accurate and simple analytic representation of the electron-gas correlation energy," Phys. Rev. B **45**, 13244 (1992).
[42]M. K. Agarwal and P. A. Wani, "Growth conditions and crystal structure parameters of layer compounds in the series $Mo_{1-x}W_xSe_2$," Mater. Res. Bull. **14**, 825–830 (1979).
[43]H. Fang, C. Battaglia, C. Carraro, S. Nemsak, B. Ozdol, J. S. Kang, H. A. Bechtel, S. B. Desai, F. Kronast, A. A. Unal, G. Conti, C. Conlon, G. K. Palsson, M. C. Martin, A. M. Minor, C. S. Fadley, E. Yablonovitch, R. Maboudian, and A. Javey, "Strong interlayer coupling in van der Waals heterostructures built from single-layer chalcogenides," Proc. Natl. Acad. Sci. U. S. A. **111**, 6198–6202 (2014).
[44]H. Nan, Z. Wang, W. Wang, Z. Liang, Y. Lu, Q. Chen, D. He, P. Tan, F. Miao, X. Wang, J. Wang, and Z. Ni, "Strong photoluminescence enhancement of MoS_2 through defect engineering and oxygen bonding," ACS Nano **8**, 5738–5745 (2014).
[45]R. Addou, C. M. Smyth, J.-Y. Noh, Y.-C. Lin, Y. Pan, S. M. Eichfeld, S. Fölsch, J. A. Robinson, K. Cho, R. M. Feenstra, and R. M. Wallace, "One dimensional metallic edges in atomically thin WSe_2 induced by air exposure," 2D Mater. **5**, 025017 (2018).
[46]T.-X. Huang, X. Cong, S.-S. Wu, K.-Q. Lin, X. Yao, Y.-H. He, J.-B. Wu, Y.-F. Bao, S.-C. Huang, X. Wang, P.-H. Tan, and B. Ren, "Probing the edge-related properties of atomically thin MoS_2 at nanoscale," Nat. Commun. **10**, 5544 (2019).
[47]W. Zhao, Z. Ghorannevis, L. Chu, M. Toh, C. Kloc, P.-H. Tan, and G. Eda, "Evolution of electronic structure in atomically thin sheets of WS_2 and WSe_2," ACS Nano **7**, 791–797 (2013).
[48]P.-C. Yeh, W. Jin, N. Zaki, D. Zhang, J. T. Liou, J. T. Sadowski, A. Al-Mahboob, J. I. Dadap, I. P. Herman, P. Sutter, and R. M. Osgood, "Layer-dependent electronic structure of an atomically heavy two-dimensional dichalcogenide," Phys. Rev. B **91**, 041407 (2015).
[49]N. R. Wilson, P. V. Nguyen, K. Seyler, P. Rivera, A. J. Marsden, Z. P. L. Laker, G. C. Constantinescu, V. Kandyba, A. Barinov, N. D. M. Hine, X. Xu, and D. H. Cobden, "Determination of band offsets, hybridization, and exciton binding in 2D semiconductor heterostructures," Sci. Adv. **3**, e1601832 (2017).
[50]J. Chang, S. Larentis, E. Tutuc, L. F. Register, and S. K. Banerjee, "Atomistic simulation of the electronic states of adatoms in monolayer MoS_2," Appl. Phys. Lett. **104**, 141603 (2014).
[51]M. Ahmad, E. Müller, C. Habenicht, R. Schuster, M. Knupfer, and B. Büchner, "Semiconductor-to-metal transition in the bulk of WSe_2 upon potassium intercalation," J. Phys.: Condens. Matter **29**, 165502 (2017).
[52]K. He, N. Kumar, L. Zhao, Z. Wang, K. F. Mak, H. Zhao, and J. Shan, "Tightly bound excitons in monolayer WSe_2," Phys. Rev. Lett. **113**, 026803 (2014).
[53]R. Schuster, Y. Wan, M. Knupfer, and B. Büchner, "Nongeneric dispersion of excitons in the bulk of WSe_2," Phys. Rev. B **94**, 085201 (2016).
[54]H. J. Liu, L. Jiao, L. Xie, F. Yang, J. L. Chen, W. K. Ho, C. L. Gao, J. F. Jia, X. D. Cui, and M. H. Xie, "Molecular-beam epitaxy of monolayer and bilayer WSe_2: A scanning tunneling microscopy/spectroscopy study and deduction of exciton binding energy," 2D Mater. **2**, 034004 (2015).
[55]C. Zhang, Y. Chen, J.-K. Huang, X. Wu, L.-J. Li, W. Yao, J. Tersoff, and C.-K. Shih, "Visualizing band offsets and edge states in bilayer-monolayer transition metal dichalcogenides lateral heterojunction," Nat. Commun. **7**, 10349 (2016).
[56]Z. Chu, A. Han, C. Lei, S. Lopatin, P. Li, D. Wannlund, D. Wu, K. Herrera, X. Zhang, A. H. MacDonald, X. Li, L.-J. Li, and K. Lai, "Energy-resolved photoconductivity mapping in a monolayer-bilayer WSe_2 lateral heterostructure," Nano Lett. **18**, 7200–7206 (2018).
[57]C. Xia, W. Xiong, J. Du, T. Wang, Y. Peng, Z. Wei, J. Li, and Y. Jia, "Type-I transition metal dichalcogenides lateral homojunctions: Layer thickness and external electric field effects," Small **14**, 1800365 (2018).
[58]Z. Jia, J. Shi, Q. Shang, W. Du, X. Shan, B. Ge, J. Li, X. Sui, Y. Zhong, Q. Wang, L. Bao, Q. Zhang, and X. Liu, "Charge-transfer-induced photoluminescence properties of WSe_2 monolayer-bilayer homojunction," ACS Appl. Mater. Interfaces **11**, 20566–20573 (2019).

© Author(s) 2020